Desiccant wheels for air humidification: An experimental and numerical analysis

Stefano De Antonellis *, Manuel Intini, Cesare Maria Joppolo, Luca Molinaroli, Francesco Romano

Dipartimento di Energia, Politecnico di Milano, Via Lambruschini, 4, 20156 Milan, Italy

Received 22 July 2015
Accepted 11 September 2015

1. Introduction

In cold climates air humidification is essential to prevent low relative humidity levels in building environments, in particular in hospitals, museums, laboratories and storage buildings. Low humidity can lead to occupants' discomfort, such as dry nose, throat, and eyes, headaches and skin irritation.

Conventional humidification devices are classified on the process imposed to the moist air that flows through them: namely adiabatic systems and isothermal systems [1]. In the adiabatic systems, the moist air undergoes a near isenthalpic process with a contemporary increase in humidity ratio and decrease in dry bulb temperature. The moist air is put in contact with liquid water, which evaporates in the air stream that directly supplies the energy required for water phase transition. On the other hand, in the isothermal system the moist air undergoes an increase in humidity ratio at almost constant dry bulb temperature. This pro-cess is achieved mixing the moist air with steam produced in appropriate equipment.

Comparing the two systems, the adiabatic humidifier is particularly diffused because it is generally cheaper and more efficient (in terms of primary energy consumption) than the isothermal one. However, in some applications the adiabatic humidifiers cannot be used due to risk of bacterial growth related to the entrainment transport of contaminated water droplets. This issue is solved with an isothermal humidifier since both the steam molecules are generally smaller than bacteria and the steam temperature is so high that it kills the pathogens. In hospital *HVAC* systems, steam humidifiers are strictly required [2] while adiabatic humidifiers are not allowed.

In the present paper, an innovative air humidification system based on a desiccant wheel is analyzed through a numerical and experimental approach. The desiccant wheel is a device obtained rolling up sheets of a supporting structure coated with a sorption material, which is crossed in counter current arrangement by two air flows [3]. Such a component is conventionally used to dehumidify an air stream in desiccant evaporative cooling (*DEC*) cycles or in industrial drying processes. Instead, in this work, it is properly integrated in an air handling unit (*AHU*) in order to humidify an air stream, by extracting water vapour from outdoor environment. The proposed system, described in detail in Section 2, is particularly suitable for hospital applications because it does not incur in air contamination risks. In fact:

- There is not presence of water droplets.
- Water vapour is adsorbed from outside air, rather than from the exhaust air stream leaving the building which can be contaminated.

* Corresponding author. Tel.: +39 0223993823; fax: +39 0223993913.
E-mail address: stefano.deantonellis@polimi.it (S. De Antonellis).

Nomenclature

a_c	channel height (mm)
A	desiccant wheel area (m^2)
A, B	experimental tests
AH	adiabatic humidifier
AHU	air handling unit
b_c	channel base (mm)
cp	specific heat (kJ kg^{-1} K^{-1})
$c1$, $c2$	adsorption isotherm equation coefficient
DEC	desiccant evaporative cooling
DWH	desiccant wheel humidification
$e1$, $e2$	adsorption isotherm equation exponents
EXP	experimental
ESH	electric steam humidifier
f	mass per unit of length (kg m^{-1})
GSR	gas side resistance
h	enthalpy (kJ kg^{-1})
h_m	heat transfer coefficient (W m^{-2} K^{-1})
h_T	mass transfer coefficient (kg m^{-2} s^{-1})
$k1$, $k2$	pressure drop equation coefficient
Le	Lewis number (–)
$\dot{m}$	mass flow rate (kg s^{-1})
N	revolution speed (rev h^{-1})
N_{test}	number of tests
Nu	Nusselt number (–)
P	channel perimeter (m)
$\dot{Q}$	power (kW)
Q_{ads}	isosteric heat of adsorption (J kg^{-1})
t	time (s)
u	measurement uncertainty
SIM	simulation
Sh	Sherwood number (–)
SSH	steam to steam humidifier
T	temperature (°C)
v	face air velocity (m s^{-1})
v'	channel air velocity (m s^{-1})
W	water content (kg kg^{-1})
x_i	measured quantity (–)
X	humidity ratio (kg kg^{-1})
y	goal function (–)
z	channel length (m)

Greek letters

ΔP	pressure drop (Pa)
ΔT	temperature difference (°C)
ΔX	humidity ratio difference (kg kg^{-1})
η	efficiency (–)
ε	calculated quantity (–)
λ	water latent heat of vaporization (kJ kg^{-1})
ρ	density (kg m^{-3})
μ	dynamic viscosity (kg m^{-1} s^{-1})
σ	wheel porosity (–)

Superscripts

EXP	experimental
SIM	simulation

Subscripts

15	at 15 °C
100	at 100 °C
a	air
ad	adsorbed water
amb	indoor ambient air conditions
AH	adiabatic Humidifier
ads	desiccant wheel sorption material
D	desiccant
DW	desiccant wheel
DWHS	desiccant wheel humidification system
e	outdoor air condition
el	electric
ESH	electric steam Humidifier
EXP	experimental
fan	fan
fil	filter
HC	heating coil
hum	humidifier
in	inlet
inst	instrument
l	liquid
max	maximum
out	outlet
p	primary source
pro	process air stream
reg	regeneration air stream
s	supply air condition
SSH	steam to steam humidifier
th	thermal
th,v	thermal – water vapour production
v	vapour
w	channel wall
x_i	measured quantity (–)

In addition, it can be driven by low temperature heat, leading to possible energy savings compared to steam humidifiers.

At present there is great interest in *DEC* cycles for air cooling and dehumidification applications. Angrisani et al. [4] analyzed a micro-trigeneration system based on a reciprocating engine and a desiccant wheel *AHU*. They put in evidence that primary energy savings can be achieved compared to conventional technologies. El-Agouz and Kabeel [5] evaluated performance of a hybrid system integrating a desiccant wheel, solar collectors and geothermal energy, showing the effects of different climates. Elgendy et al.[6] discussed the effect of different evaporative cooling arrangements in desiccant wheel based *AHU*. Liu et al. [7] evaluated the integration of a desiccant wheel with existing technologies and discussed the importance of operating conditions on system performance. Ruivo et al. [8] recently investigated the importance of desiccant wheel modeling in energy system simulations, highlighting that simplified approaches lead to questionable results.

Further studies deal with the use of desiccant wheels for drying in food industry. De Antonellis et al. [9] investigated different system configurations and highlighted the optimal solutions as a function of sensible to latent heat ratio and ambient conditions. Dai et al. [10] evaluated performance of a system coupling solar collectors and a desiccant wheel, showing it is suitable for grain drying in regions with high solar irradiation. Wang et al. [11] showed that desiccant wheel systems can be effectively used for air drying in food industry packaging. Guan et al. [12] evaluated that energy efficiency in steel plants is increased by using desiccant wheels to dry and pre-heat air for blast furnace. It has been investigated that COP of refrigerating chillers can be improved by the integra-tion with a desiccant wheel in case of a trans-critical CO_2 cycle

by Aprea et al. [13] and of a conventional cycle by Sheng et al. [14]. Finally Fong et al. [15] put in evidence that a system composed of a desiccant wheel, an absorption chiller and solar collectors can lead to energy savings compared to the reference technology in case of subtropical climate.

Substantially there is lack of studies about the use of desiccant wheels for air humidification. La et al. [16] and Zeng et al. [17] investigated a solar heating and humidification system with a one-rotor two-stage desiccant device. Outside air is provided to the building environment while return air is used as moisture source. The first work [16] mainly deals with the experimental and theoretical analysis of the system while the second one [17] deals with its numerical optimization. They highlighted the system can improve occupants' comfort due to the increase in relative humidity, which is not strictly controlled, compared to an equivalent system without desiccant rotor. Anyway this configuration is not suitable for applications where contamination between fresh and exhaust air is not acceptable, such as in hospital buildings [18].

Referring to the aforementioned state of the art, the aim of this work is:

1. To investigate the use of desiccant wheels to humidify an air stream by extracting moist from outside air.
2. To experimentally analyze the performance of the proposed system.
3. To evaluate the effects of boundary conditions on humidification capacity and to design the best system configuration through a phenomenological desiccant wheel model based on heat and mass transfer equations.

2. Description of the proposed air humidification system

The proposed air humidification system is shown in Fig. 1. It is crossed by two air streams, namely the regeneration and the process one and consists of the following components:

- A desiccant wheel.
- Two heating coils.
- Two fans.
- Two filters.

According to the terminology conventionally adopted in *DEC* cycle, the process air stream is heated and dehumidified across the desiccant wheel while the regeneration air flow is cooled and humidified. Despite of conventional *DEC* cycles, in this case the useful effect is evaluated on the regeneration air stream side. A scheme of the system and air treatments are respectively reported in Figs. 1 and 2.

Both air streams entering the system are assumed to be at outside temperature and humidity conditions (E). The regeneration air is first heated through a heating coil ($E-1$), then it is cooled and humidified across the desiccant wheel (1–2) and finally it is heated

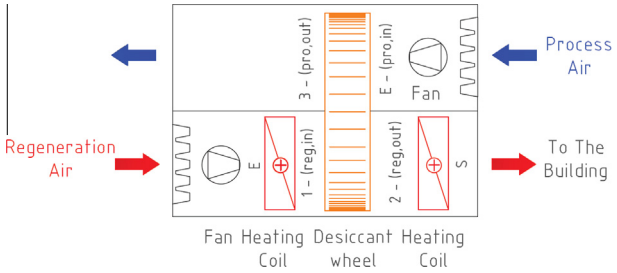

Fig. 1. Scheme of the proposed air humidification system.

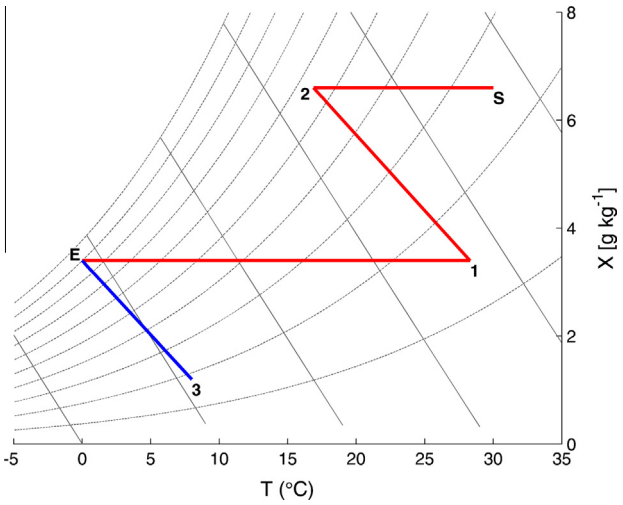

Fig. 2. Representation of air transformations of the proposed humidification system in the psychrometric chart.

to the desired temperature through the second coil ($2-S$), before being supplied to the air conditioned building. The process air flow is heated and dehumidified ($E-3$) and exhausted to the outside environment.

3. Adopted methodologies

The analysis reported in this work has been performed through the following approach:

1. A desiccant wheel has been tested in a laboratory facility. Measurements have been carried out in representative working conditions of the proposed humidification system, which are significantly different from the ones of conventional *DEC* cycles.
2. A detailed desiccant wheel model previously developed [3], based on heat and mass transfer equations, has been calibrated in order to properly match a subset of experimental data.
3. Results of the calibrated model have been compared to further experimental data, which have not been used in the calibration process, in order to verify the validity of the model.
4. Simulations are performed to evaluate the optimal system configuration, the effect of boundary conditions and off design performance.
5. The power consumption, referred to the primary source of the proposed humidification system, has been compared to the one of reference technologies.

3.1. Test facility and investigated desiccant wheel

The test rig, which has been deeply described in previous works [19,20], consists of two air handling units designed to properly control temperature, humidity and mass flow rate of both air streams (Fig. 3). Air conditions are controlled through heating coils, cooling coils and evaporative coolers. In addition in the regeneration air stream unit an electrical heater is installed, in order to rise the flow temperature up to 100 ° C. Air flow rates are controlled by variable speed fans and each one is measured through two orifice plates, constructed according to technical standards [21] and installed in two different parallel ducts. Pressure drop across the orifices and across the desiccant wheel is measured by piezoelectric transmitters. The maximum process air flow rate is 2000 $m^3\ h^{-1}$ and the maximum regenera-tion air flow rate is 1400 $m^3\ h^{-1}$.

Fig. 3. Air handling units of the test rig.

The desiccant wheel is crossed in counter-current arrangement by the two air streams (Fig. 4). Its casing is made of chipboards insulated with polystyrene panels (30 mm thickness). Temperature and relative humidity of each air stream are measured at the inlet and outlet section of the casing with coupled RTD PT100 and humidity capacitive sensors, as summarized in Table 1.

The tested desiccant wheel is made of synthesized metal silicate on inorganic fibre substrate, whose adsorption isotherm shows a Type IV trend [20] according to the IUPAC classification [22]. The outer diameter of the commercial device is 60 cm and its axial length is 20 cm. Channels have a sinusoidal cross sectional area with height equal to 1.8 mm and base equal to 3.55 mm. The component is split in two equal sections without any purge sector.

For each test, experimental data are collected in steady state conditions and in each session at least 300 samples of every physical quantity have been logged with a frequency of 1 Hz.

The experimental uncertainty u_{xi} is estimated according to Moffat [23]:

$$u_{x_i} = \pm\sqrt{u_{x_{i,inst}}^2 + \left(t_{95}\ \sigma_{\overline{x_i}}\right)^2} \tag{1}$$

where $u_{xi,inst}$ is the instrument uncertainty of the generic measured parameter, t_{95} is the student test multiplier at 95% confidence and $\sigma_{\overline{x_i}}$ is the standard deviation of the mean. The generic combined uncertainty u_ε of calculated quantities ε, is calculated as:

$$u_\varepsilon = \sqrt{\sum_i \left(\frac{\partial \varepsilon}{\partial x_i} u_{x_i,inst}\right)^2 + t_{95}^2 \sum_i \left(\frac{\partial \varepsilon}{\partial x_i} \sigma_{\overline{x_i}}\right)^2} \tag{2}$$

Table 1
Sensors main data.

Abbreviation	Type of sensor	Accuracy[a]
T[b]	PT 100 Class A	±0.2 °C
RH[b]	Capacitive	±1% (between 0% and 90%)
p	Piezoelectric	±0.5% of reading ±1 Pa

[a] At T = 20 °C.
[b] Temperature and relative humidity probe.

3.2. Model description and calibration

The present study has been carried out through a one-dimensional gas side resistance (*GSR*) model, which has been described in detail in a previous work [3]. Main assumptions of the physical model are: (i) one-dimensional air flow; (ii) uniform air conditions at each inlet face of the wheel; (iii) negligible heat and mass transfer between adjacent channels and to the surround-ings; (iv) negligible axial heat conduction and water vapour diffu-sion in the air stream and in the desiccant material; (v) negligible air leakages between the air streams. The following equations have been applied to an infinitesimal element of the channel.

Energy and water mass conservation in the desiccant material and adsorbed water:

$$(f_D\, cp_D + f_D c_{ad} W_D)\frac{\partial T_D}{\partial t} = (cp_v(T_a - T_D) + Q_{ads})h_m(X - X_w)\, P + h_T(T_a - T_D)P \tag{3}$$

$$\frac{\partial W_D}{\partial t} = \frac{h_m(X - X_w)\, P}{f_D} \tag{4}$$

Energy, water mass and dry air mass conservation in the air stream:

$$\frac{\partial T_a}{\partial t} = -v'\frac{\partial T_a}{\partial z} - \frac{h_T\,(T_a - T_D)\,P}{cp_a\,\rho_a\,A} - \frac{h_m\,(X - X_W)Pcp_vT_a}{cp_a\,\rho_a\,A} \tag{5}$$

$$\frac{\partial X}{\partial t} = -\frac{\partial X}{\partial z}v' - \frac{P\,h_m}{\rho_a A}(X - X_w) \tag{6}$$

$$\frac{\partial \rho_a}{\partial t} = -\frac{\partial(\rho_a v')}{\partial z} \tag{7}$$

A detailed description of Eqs. (3)–(7), boundary and initial conditions and closure equations are reported in [3].

Main desiccant wheel data have been measured or collected from the manufacturer while two parameters, namely cp_D and f_D, have been fitted from experimental tests of the desiccant wheel, as summarized in Table 2. A sample of the desiccant wheel sorp-tion and substrate material has been collected in order to measure the adsorption isotherm at 50 °C with a dynamic vapour sorption

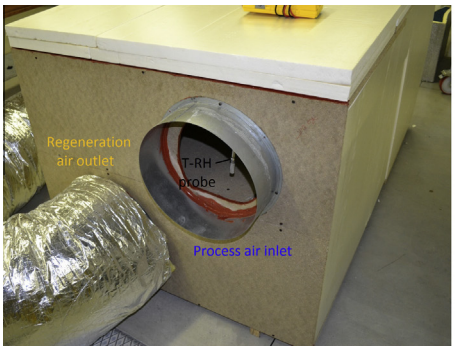

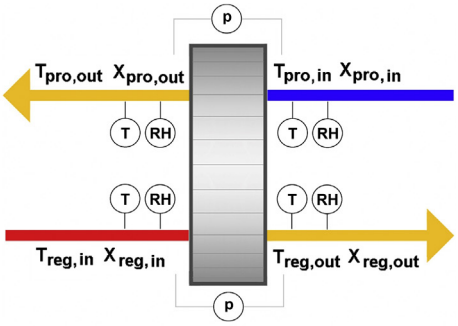

Fig. 4. Desiccant wheel casing and scheme, with indication of installed sensors.

Table 2
Desiccant wheel parameters.

Parameter	Value	
a_c	1.80	(mm)
b_c	3.55	(mm)
Nu	2.1	(–)
σ	0.76	(–)
c_1	2.28	(–)
c_2	213.40	(–)
e_1	0.97	(–)
e_2	5.67	(–)
cp_D[a]	2.64	(kJ kg^{-1} K^{-1})
f_D[a]	0.00040	(kg m^{-1})

[a] Fitted according to goal function of Eq. (9).

analyzer [20]. The adsorption isotherm has been fitted through a polynomial equation:

$$\phi = c_1 W_D^{e1} + c_2 W_D^{e2} \tag{8}$$

Based on the channel dimensions reported in Table 2, the aspect ratio a_c/b_c is equal to 0.51 and therefore the Nusselt number in fully developed laminar flow condition and at constant wall temperature is $Nu \approx 2.1$.

The isosteric heat of adsorption has been assumed equal to the latent heat of water. No information about the specific heat and the amount of support and sorption material was available. According to the detailed analysis reported by Aprile and Motta [24], a Grey-box approach has been adopted to evaluate unknown values of desiccant wheel properties. Two sets of tests, *A*1 and *B*1 (Table 3), have been used to evaluate appropriate values of cp and f_D. The pair of values that minimize the following goal function has been adopted in the model:

$$y = \sum_{i=1}^{N_{test}} \left(\frac{\left(X_{pro,out}^{SIM} - X_{pro,in}\right) - \left(X_{pro,out}^{EXP} - X_{pro,in}\right)}{X_{pro,out}^{EXP} - X_{pro,in}} \right)^2 + \sum_{i=1}^{N_{test}} \left(\frac{\left(T_{pro,out}^{SIM} - T_{pro,in}\right) - \left(T_{pro,out}^{EXP} - T_{pro,in}\right)}{T_{pro,out}^{EXP} - T_{pro,in}} \right)^2 \tag{9}$$

where superscripts *SIM* and *EXP* refer respectively to the numeric simulations and to the experimental tests and subscripts $_{pro,in}$ and $_{pro,out}$ refer respectively to the process air inlet and outlet. Since outlet temperature and humidity ratio should be properly estimated by the mathematical model, both of them have been included in the proposed goal function. Process air conditions have been selected to evaluate the goal function due to their lower uncertainty compared to the regeneration ones. As a result of the adopted approach, f_D is equal to 4.0×10^{-4} kg m^{-1} and cp_D is equal to 2.64 kJ kg^{-1} K^{-1}.

In Table 3 experimental and numerical outlet air conditions are reported. Relative error between predicted and measured values of ΔX_{pro}, ΔX_{reg}, ΔT_{pro} and ΔT_{reg} across the desiccant wheel are always within ±11%. More precisely, the relative error between simulated and experimental values is within 56.3% in 5% of cases and within 10% in 84.4% of cases.

3.3. Experimental and numerical results

After the model calibration performed through data *A*1 and *B*1, simulation results have been compared with additional experimental tests *A*2 and *B*2 (Table 4). Outlet air conditions of both process and regeneration air streams are reported as a function of regeneration temperature and revolution speed, respectively in Figs. 5 and 6 and in Figs. 7 and 8. Numerical results and experimental data are plotted both for tests adopted in the calibration process (*A*1 and *B*1) and for the additional ones (*A*2 and *B*2). Boundary conditions of all tests are representative of the ones that can be reached in the proposed humidification system. In tests *A*2 process air flow rate has been increased by 50% compared to tests *A*1. Instead, in tests *B*2 process air flow rate and both inlet humidity ratio have been reduced compared to tests *B*1. It is highlighted that experiments at lower inlet humidity ratio (2–3 g kg^{-1}) and process air temperature (<10 °C) have not been performed due to technical limitations of the test rig. As shown in Figs. 5–8, the model is able to properly predict the trend of experimental data in a wide range of operating conditions.

Table 3
Experimental data used to calibrate the desiccant wheel model.

Test (–)	Inlet							Experimental outlet				Numerical outlet[a]			
	$T_{pro,in}$ (°C)	$X_{pro,in}$ (g kg^{-1})	$v_{pro,in}$ (m s^{-1})	$T_{reg,in}$ (°C)	$X_{reg,in}$ (g kg^{-1})	$v_{reg,in}$ (m s^{-1})	N (rev h^{-1})	$T_{pro,out}$ (°C)	$X_{pro,out}$ (g kg^{-1})	$T_{reg,out}$ (°C)	$X_{reg,out}$ (g kg^{-1})	$T_{pro,out}$ (°C)	$X_{pro,out}$ (g kg^{-1})	$T_{reg,out}$ (°C)	$X_{reg,out}$ (g kg^{-1})
*A*1	11.9	4.5	1.90	35.1	4.6	1.87	15.5	22.1	2.2	24.6	7.3	21.8	2.3	24.3	7.0
*A*1	12.0	4.5	1.90	42.5	4.7	1.85	15.5	25.1	1.7	28.3	7.9	24.5	1.9	28.3	7.7
*A*1	12.7	4.6	1.90	48.6	4.8	1.87	15.5	27.7	1.3	31.4	8.5	27.3	1.6	32.0	8.2
*A*1	12.4	4.5	1.89	55.0	4.8	1.89	15.5	30.3	0.9	35.8	8.6	29.3	1.3	35.7	8.5
*A*1	12.9	4.5	1.89	66.0	4.8	1.94	15.5	35.0	0.6	42.6	8.8	33.3	1.0	42.6	8.9
*B*1	11.9	4.4	2.32	39.7	4.6	1.86	6.0	20.5	1.6	28.2	8.1	20.0	1.9	28.8	8.0
*B*1	11.6	4.2	2.33	40.7	4.5	1.85	10.5	20.8	1.4	27.9	7.9	21.2	1.7	27.6	8.0
*B*1	11.5	4.2	2.32	39.8	4.5	1.85	15.5	22.3	1.7	26.0	7.7	21.8	1.9	25.7	7.6

[a] Numerical outlet conditions are calculated through the calibrated model (parameters reported in Table 2).

Table 4
Experimental data and numerical input adopted in Figs. 5–8.

Test (–)	Experimental inlet							Numerical inlet						
	$T_{pro,in}$ (°C)	$X_{pro,in}$ (g kg^{-1})	$v_{pro,in}$ (m s^{-1})	$T_{reg,in}$ (°C)	$X_{reg,in}$ (g kg^{-1})	$v_{reg,in}$ (m s^{-1})	N (rev h^{-1})	$T_{pro,in}$ (°C)	$X_{pro,in}$ (g kg^{-1})	$v_{pro,in}$ (m s^{-1})	$T_{reg,in}$ (°C)	$X_{reg,in}$ (g kg^{-1})	$v_{reg,in}$ (m s^{-1})	N (rev h^{-1})
*A*1	11.9–12.9	4.5–4.6	1.89–1.90	35.1–66.0	4.6–4.8	1.85–1.94	15.5	12.0	4.5	1.90	34.0–66.0	4.8	1.90	15.5
*B*1	11.5–11.9	4.2–4.4	2.32–2.33	39.7–40.7	4.5–4.6	1.85–1.86	6–15.5	11.8	4.3	2.30	40.0	4.5	1.90	5–19
*A*2	11.5–14.9	3.9–4.2	2.71–2.72	31.9–53.2	4.1–4.5	1.85–1.92	15.5	12.0	4.1	2.70	30.0–54.0	4.3	1.90	15.5
*B*2	12.8–13.6	3.5	2.11	37.6–39.7	3.6–3.7	1.85	6–15.5	13.0	3.5	2.10	39.0	3.6	1.85	5–19

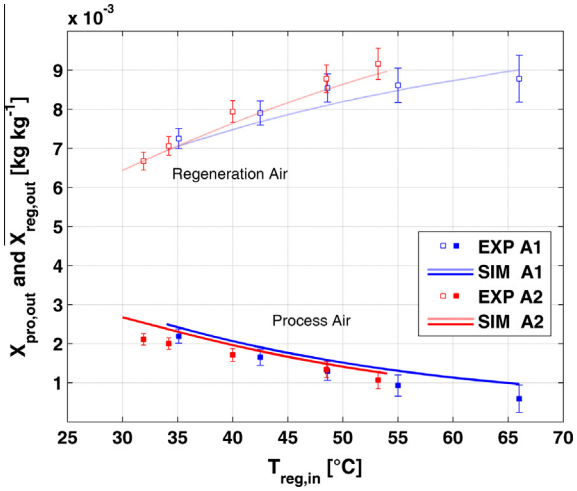

Fig. 5. Experimental and numerical outlet process and regeneration air humidity ratio in tests *A*1 and *A*2.

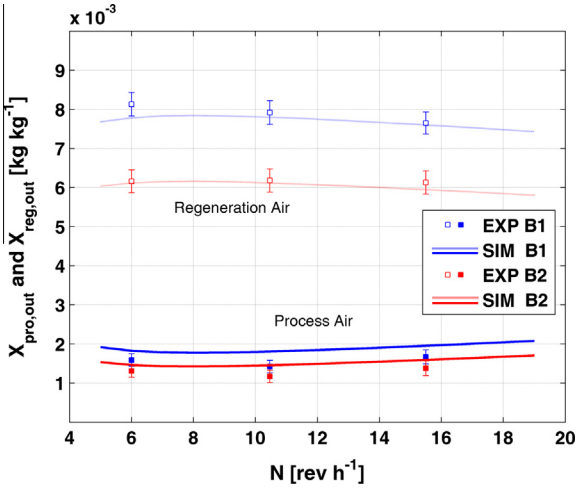

Fig. 7. Experimental and numerical outlet process and regeneration air humidity ratio in tests *B*1 and *B*2.

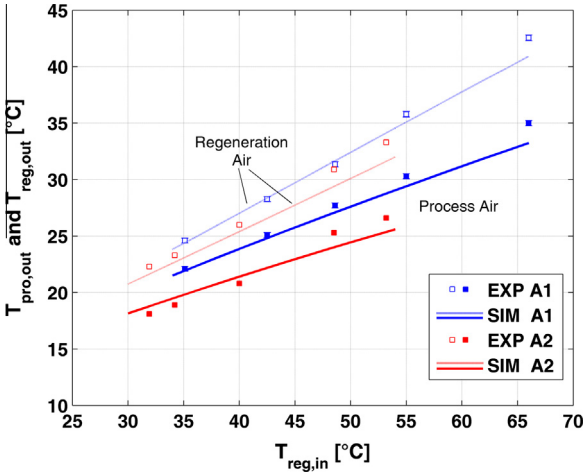

Fig. 6. Experimental and numerical outlet process and regeneration air temperature in tests *A*1 and *A*2.

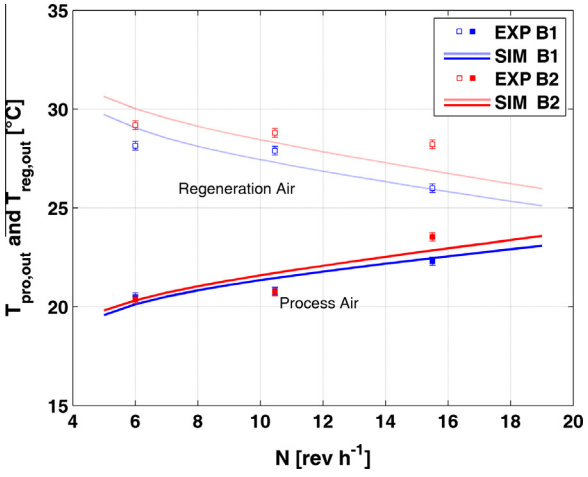

Fig. 8. Experimental and numerical outlet process and regeneration air temperature in tests *B*1 and *B*2.

4. Design and analysis of the proposed humidification system

4.1. Reference conditions

The analysis of the humidification system provided in this work is based on the following assumptions:

- The outside air temperature and humidity ratio in winter peak conditions are respectively $T_e = 0$ °C and $X_e = 3.4$ g kg^{-1}. These values can be representative of climate conditions of Southern Europe, and in particular of the centre of Italy. Further considerations about the variation of outside air temperature and humidity are reported in Section 5.
- The humidification system provides outdoor air to a hospital, whose ambient conditions are $T_{amb} = 22$ °C and $X_{amb} = 6.6$ g kg^{-1} (according to technical guidelines UNI 10339 [25]).
- The humidity ratio of the supplied air stream is $X_s = X_{reg,out} = 6.6$ g kg^{-1} (assuming negligible latent load in the building). Different values of $X_{reg,out}$ are discussed in Section 6.
- The reference value of the regeneration air face velocity on the desiccant wheel is $v_{reg,in}$ 2 m s^{-1}, which is a typical value adopted in this technology. Instead $v_{pro,in}$ has been set to 2 m s^{-1} and increased up to 3 m s^{-1}, as explained in detail in Section 4.2.

The aforementioned working conditions ($v_{reg,in} = 2$ m s^{-1}, $X_e = X_{pro,in} = X_{reg,in} = 3.4$ g kg^{-1}) have been adopted in all the figures reported in this section (Figs. 9–14).

4.2. Sensitivity analysis

In Fig. 9, $X_{reg,out}$ and $T_{reg,out}$ are plotted as a function of $T_{reg,in}$ and $v_{pro,in}$ when the outside air temperature is $T_e = 0$ °C and the humidity ratio is $X_e = 3.4$ g kg^{-1}. Quite obviously, at a given face velocity an increase in $X_{reg,in}$ leads to an increase in the outlet regeneration air humidity ratio. The process air stream ideally can be dehumidified down to the minimum value $X_{pro,out} = 0$ g kg^{-1}, and therefore also a maximum value $X_{reg,out,max}$ exists, which can be calculated in this form:

$$X_{reg,out,max} = X_{reg,in} + \frac{\dot{m}_{pro}\, X_{pro,in}}{\dot{m}_{reg}} \tag{10}$$

The aforementioned issue can be overcome by increasing the process air flow rate $\dot{m}_{pro}$, which allows to reach a higher $X_{reg,out}$ at constant inlet regeneration air temperature. Generally, as long

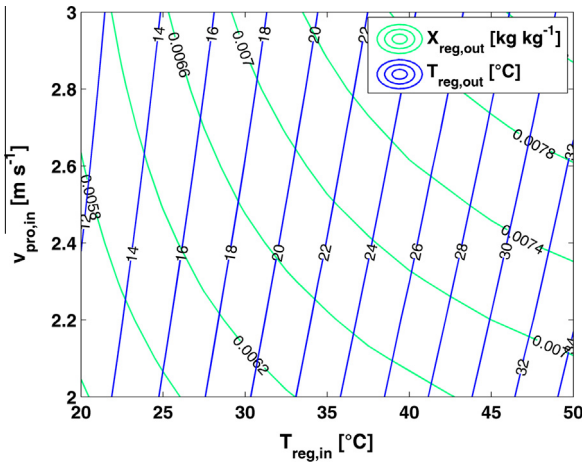

Fig. 9. $X_{reg,out}$ and $T_{reg,out}$ as a function of $T_{reg,in}$ and $v_{pro,in}$ at $T_e = T_{pro,in,} = 0$ °C and $N = 8$ rev h^{-1}.

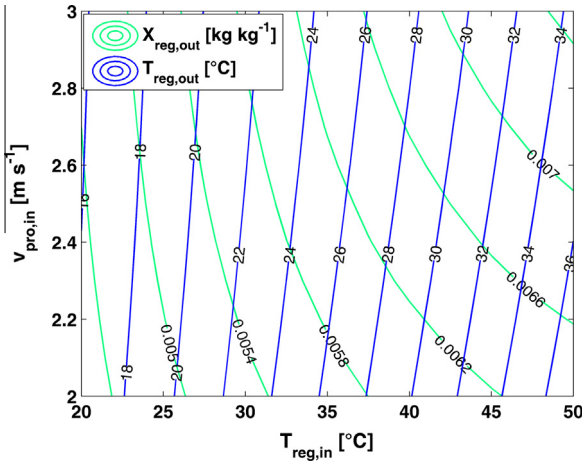

Fig. 10. $X_{reg,out}$ and $T_{reg,out}$ as a function of $T_{reg,in}$ and $v_{pro,in}$ at $T_e = T_{pro,in,} = 10$ °C and $N = 8$ rev h^{-1}.

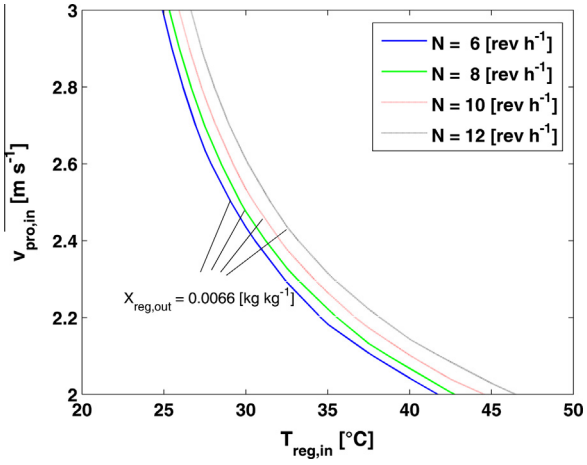

Fig. 11. $X_{reg,out}$ as a function of $T_{reg,in,}$ $v_{pro,in}$ and N at $T_e = T_{pro,in,} = 0$ °C.

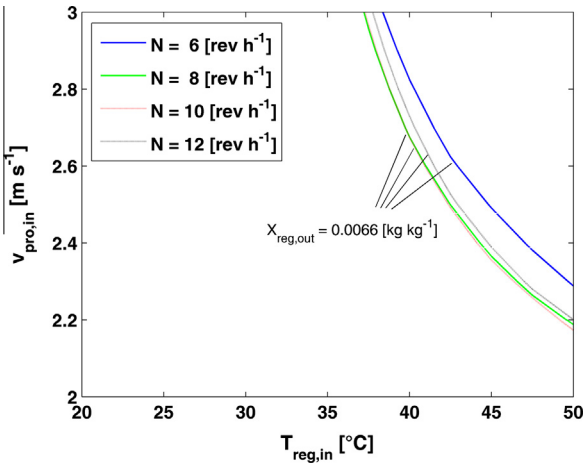

Fig. 12. $X_{reg,out}$ as a function of $T_{reg,in,}$ $v_{pro,in}$ and N at $T_e = T_{pro,in,} = 10$ °C.

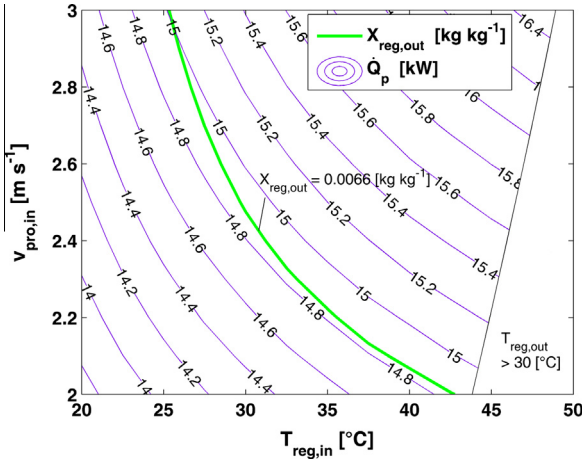

Fig. 13. $\dot{Q}_p$ as a function of $T_{reg,in}$ and $v_{pro,in}$ at $T_e = T_{pro,in,} = 0$ °C and $N = 8$ rev h^{-1}.

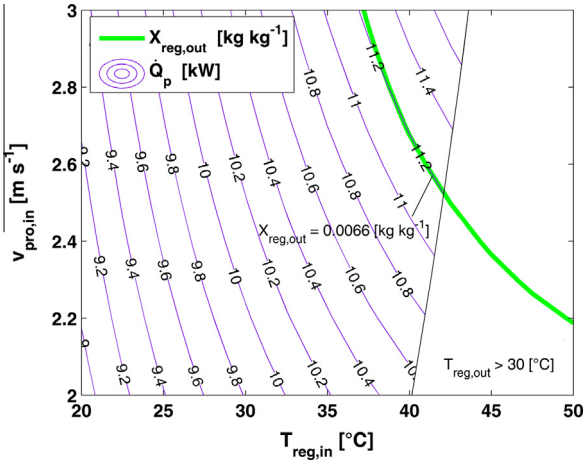

Fig. 14. $\dot{Q}_p$ as a function of $T_{reg,in}$ and $v_{pro,in}$ at $T_e = T_{pro,in,} = 10$ °C and $N = 8$ rev h^{-1}.

as $X_{reg,out} < X_{reg,out,max}$, the desired value of outlet regeneration air humidity ratio can be achieved either by the variation of $v_{pro,in}$ or $T_{reg,in}$. It is highlighted that the higher the inlet regeneration temperature, the higher the outlet regeneration temperature: this effect is discussed in detail in Section 4.3.

In Fig. 10 the trend of $X_{reg,out}$ and $T_{reg,out}$ are shown when $T_e = T_{pro,in,} = 10$ °C. At constant $X_{pro,in}$, the higher $T_{pro,in}$ the lower

$\varphi_{pro,in}$. As a result, the desiccant wheel dehumidification capacity decreases [3] and therefore $X_{pro,out}$ and $X_{reg,out}$ respectively increases and reduces. According to the aforementioned considerations, if T_e = 10 °C (Fig. 10) at a given $v_{pro,in}$ the target $X_{reg,out}$ = 6.6 g kg^{-1} is reached at a higher inlet regeneration temperature, compared to the case at T_e = 0 °C (Fig. 9). Therefore, in the design of the proposed humidification system, it should be carefully considered that the most critical working condition is not at the lowest outside temperature and humidity ratio, but it occurs when the temperature rises at low humidity ratio.

In Figs. 11 and 12, it is shown the relationship between the revolution speed and the target $X_{reg,out}$ = 6.6 g kg^{-1}: the optimal values are N = 6 rev h^{-1} when T_e = 0 °C and N = 8 rev h^{-1} when T_e = 10 °C. In the second case, the target $X_{reg,out}$ = 6.6 g kg^{-1} is reached at higher regeneration temperature compared to the previous one. According to Intini et al. [26], the increase in N can be explained considering that the higher the regeneration temperature, the higher the optimal revolution speed.

4.3. Optimal configuration

According to the considerations reported in Sections 4.1 and 4.2, the proposed desiccant wheel humidification system (*DWH*) is designed in order to humidify the regeneration air stream up to $X_{reg,out}$ = 6.6 g kg^{-1} with T_e = 10 °C, X_e = 3.4 g kg^{-1}, $v_{reg,in}$ = 2 m s^{-1} and N = 8 rev h^{-1}. It is put in evidence that different values of T_e could be assumed, considering that the higher T_e, the higher the regeneration temperature. Therefore the analysis of the local climate data, which is not the aim of the present work, should be carefully performed before the design of the system.

In order to make all the investigated configurations directly comparable, a constant supply air temperature T_s = 30 °C has been chosen. A higher temperature has not been selected to avoid discomfort conditions in the building [27].

The best pair $T_{reg,in}$ and $v_{pro,in}$ is selected in order to minimize the power consumption referred to primary source in separated power production. $\dot{Q}_{p,DWH}$ is calculated in this form:

$$\dot{Q}_{p,DWH} = \frac{\dot{Q}_{th,DWH}}{\eta_{th}} + \frac{\dot{Q}_{el,DWH}}{\eta_{el}} \tag{11}$$

where referring to Fig. 1:

$$\dot{Q}_{th,DWH} = \dot{m}_{reg} cp_a \left[\left(T_{reg,in} - T_e \right) + \left(T_s - T_{reg,out} \right) \right] \tag{12}$$

$$\dot{Q}_{el,DWH} = \left(\Delta P_{fil} + \Delta P_{DW,reg} + 2\Delta P_{HC} \right) \frac{v_{reg,in} A_{reg}}{\eta_{fan}} + \left(\Delta P_{fil} + \Delta P_{DW,pro} \right) \frac{v_{pro,in} A_{pro}}{\eta_{fan}} \tag{13}$$

The regeneration air mass flow rate is $\dot{m}_{reg} = v_{reg,in} A_{reg} \rho_{reg}$ and the values used in Eqs. (11)–(13) are summarized in Table 5.

Note that A_{pro} and A_{reg} refer to the actual dimensions of the tested desiccant wheels.

Table 5
Parameters used in the calculation of power consumption of the proposed humidification system.

Parameter	Value
A_{pro} (m^2)	0.132
A_{reg} (m^2)	0.132
ΔP_{fil} (Pa)	150
ΔP_{HC} (Pa)	50
η_{fan} (–)	0.7
η_{th} (–)	0.9
η_{el} (–)	0.525

Pressure drop across the desiccant wheel are calculated according to the correlation provided by De Antonellis et al. [20] for the same desiccant wheel:

$$\Delta P_{DW} = k_1 \mu_a \, v_a + k_2 \rho_a v_a^2 \tag{14}$$

With $k_1 = 3.77 \times 10^6$ and k_2 = 6.5493.

Simulation results are reported in Figs. 13 and 14 respectively at T_e = 0 °C and T_e = 10 °C. In the second condition values of $\dot{Q}_p$ are lower due to the higher outside temperature and, therefore, the lower heating load. In case of low values of $v_{pro,in}$, (2 m s^{-1}), the tar-get humidity ratio $X_{reg,out}$ = 6.6 g kg^{-1} is achieved with high $T_{reg,in}$ (>40 °C if T_e = 10 °C), which leads to high $T_{reg,out}$. Such a tempera-ture can be easily higher than 30 °C, which has been selected as maximum condition in this analysis in order to prevent discomfort in the building. In Figs. 13 and 14, the values of $\dot{Q}_p$ in case of $T_{reg,out}$ is higher than 30 °C have not been represented. Note that values of $T_{reg,out}$ have already been shown in Figs. 9 and 10.

On the other side, an increase in $v_{pro,in}$ leads to a slight increase in $\dot{Q}_p$. In conclusion, there are many pairs $T_{reg,in}$ and $v_{pro,in}$ that allow to reach the target $X_{reg,out}$ = 6.6 g kg^{-1} and a trade-off between high $T_{reg,out}$ or high $\dot{Q}_p$ should be found. A possible satisfactory configuration, which is adopted in the following of this study, is reached through the pair $v_{pro,in}$ = 2.6 m s^{-1} and $T_{reg,in}$ = 40 °C when T_e = 10 °C and X_e = 3.4 g kg^{-1} (Fig. 14).

5. Off design performance analysis

In this section the effect of the variation of X_e and T_e on the performance of the proposed humidification system are investigated. As reported in Fig. 15, if X_e reduces at constant T_e, the desiccant wheel regeneration temperature should be increased in order to reach a desired $X_{reg,out}$. As expected, it is possible that a target $X_{reg,out}$ cannot even be reached: for example if X_e = 2.4 g kg^{-1} and T_e = 0 °C, the maximum achievable $X_{reg,out,max}$ is lower than 6.6 g kg^{-1}. Therefore in this case the adopted configuration is not still satisfactory and a new one, with higher process air flow rate, should be chosen. On the opposite, if X_e increases at constant T_e, the target $X_{reg,out}$ is reached with a lower regeneration temperature and, consequently, with a lower $T_{reg,out}$ (Fig. 16).

It is possible to state that peak conditions used to design the system should be carefully selected, in order to avoid working condition that cannot be satisfied by the humidification system.

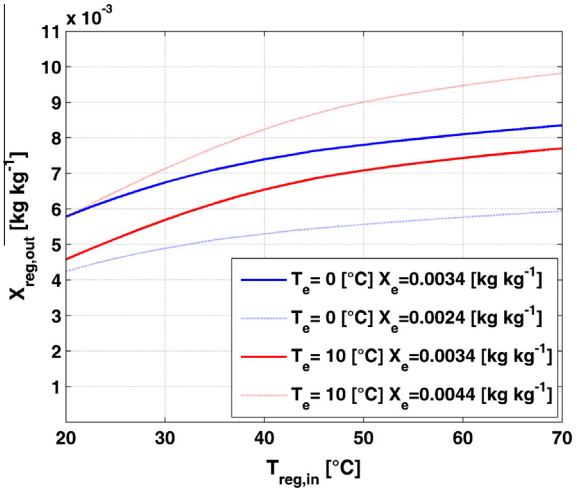

Fig. 15. $X_{reg,out}$ as a function of $T_{reg,in}$ for different T_e and X_e ($v_{reg,in}$ = 2 m s^{-1}, $v_{pro,in}$ = 2.6 m s^{-1}, N = 8 rev h^{-1}).

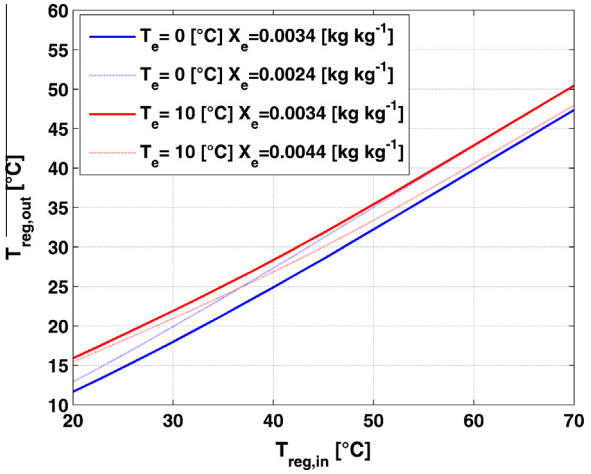

Fig. 16. $T_{reg,out}$ as a function of $T_{reg,in}$ for different T_e and X_e ($v_{reg,in}$ = 2 m s^{-1}, $v_{pro,in}$ = 2.6 m s^{-1}, N = 8 rev h^{-1}).

6. Comparison with reference humidification technologies

In this section, the proposed desiccant wheel humidification (*DWH*) system is compared to conventional technologies in terms of power consumption referred to the primary source (separated power production). Four reference technologies are analyzed:

- An adiabatic humidifier (*AH*).
- An electric steam humidifier (*ESH*).
- Two steam to steam humidifiers (*SSH* 1 and *SSH* 2).

In the conventional adiabatic humidifier water evaporation occurs: in this case $\dot{Q}_p$ is calculated only as a benchmark because such as system cannot be compared to the investigated technology due to contamination issues, as described in detail in Section 1. In *ESH* water vapour is generated through electrodes or thermal resistances while in *SSH* water vapour is generated through steam produced in a specific boiler. In this last case, two different boiler efficiencies, defined including also overall piping heat losses, have been considered in the analysis (*SSH* 1 and *SSH* 2).

The terms $\dot{Q}_p$, $\dot{Q}_{th}$ and $\dot{Q}_{el}$ of the proposed humidification sys-tem based on desiccant wheel are calculated through Eqs. (11)–(13). Instead, power consumption of the reference humidification technologies is determined with Eqs. (15)–(24), as reported in the following.

Adiabatic humidifier:

$$\dot{Q}_{p,AH} = \frac{\dot{Q}_{th,AH}}{\eta_{th}} + \frac{\dot{Q}_{el,AH}}{\eta_{el}} \tag{15}$$

where $\dot{Q}_p$ is the power consumption referred to the primary source, $\dot{Q}_{th}$ is the thermal power consumption and $\dot{Q}_{el}$ is the electric power consumption. η_{el} and η_{th} are the reference efficiency values for the separated generation of electricity and heat.

$$\dot{Q}_{th,AH} = \dot{m}_a(h_s - h_E) \tag{16}$$

$$\dot{Q}_{el,AH} = (\Delta P_{fil} + \Delta P_{hum} + 2\Delta P_{HC})\frac{\dot{m}_a}{\rho_a \eta_{fan}} \tag{17}$$

where $\dot{m}_a$ is the mass flow rate of the air stream supplied to the building and h_s and h_E are respectively the wet air enthalpy at supply and outdoor conditions. In addition ΔP_{fil}, ΔP_{hum} and ΔP_{HC} are the pressure drop across the filter, the humidifier and the heating coils (pre and post heating) and η_{fan} is the fan efficiency.

Electric steam humidifier:

$$\dot{Q}_{p,ESH} = \frac{\dot{Q}_{th,ESH}}{\eta_{th}} + \frac{\dot{Q}_{el,ESH}}{\eta_{el}} \tag{18}$$

$$\dot{Q}_{th,ESH} = \dot{m}_a(h_s - h_E) - \dot{m}_a(X_s - X_E)\, h_{v,100} \tag{19}$$

$$\dot{Q}_{el,ESH} = (\Delta P_{fil} + \Delta P_{hum} + \Delta P_{HC})\frac{\dot{m}_a}{\rho_a \eta_{fan}} + \dot{m}_a(X_s - X_E)(h_{v,100} - h_{l,15}) \tag{20}$$

where the term $\dot{m}_a\,(X_s - X_E)\,h_{v,100}$ is the heat provided to the air stream by the steam and the term $\dot{m}_a\,(X_s - X_E)\,(h_{v,100} - h_{l,15})$ is the power consumption required to generate the steam from liquid water.

Steam to steam humidifier:

$$\dot{Q}_{p,SSH} = \frac{\dot{Q}_{th,SSH}}{\eta_{th}} + \frac{\dot{Q}_{th,v,SSH}}{\eta_{th,v}} + \frac{\dot{Q}_{el,SSH}}{\eta_{el}} \tag{21}$$

$$\dot{Q}_{th,SSH} = \dot{m}_a[h_s - h_E - h_{v,100}(X_s - X_E)] \tag{22}$$

$$\dot{Q}_{th,v,SSH} = \dot{m}_a(X_s - X_E)(h_{v,100} - h_{l,15}) \tag{23}$$

$$\dot{Q}_{el,SSH} = (\Delta P_{fil} + \Delta P_{hum} + \Delta P_{HC})\frac{\dot{m}_a}{\rho_a \eta_{fan}} \tag{24}$$

where $\dot{Q}_{th,v}$ is thermal power required to generate the primary steam flow that is used to produce the water vapour stream used in the humidification process. Note that $h_{v,100}$ and $h_{l,15}$ are the enthalpy respectively of saturated steam at 100 °C and of liquid water at 15 °C. Instead $\dot{m}_a$ is the mass flow rate of air stream sup-plied to the building, assumed $\dot{m}_a = \dot{m}_{reg}$. In Eqs. (20) and (23) it has been assumed the steam production is obtained with unitary efficiency. Data used in Eqs. (15)–(24) are summarized in Table 6.

Simulation results are reported in Fig. 17 for two working condition: T_e = 0 °C and T_e = 10 °C with X_e = 3.4 g kg^{-1}. Primary power consumption of *DWH* is always lower than *ESH* (respectively −0.47 kW and −0.26 kW at T_e = 0 °C and T_e = 10 °C) and higher than *SSH* configuration. More precisely, if $\eta_{th,v}$ = 0.8 the additional primary power consumption of *DWH* is 1.19 and 1.34 kW and if $\eta_{th,v}$ = 0.6 it is 0.11 and 0.30 kW. In order to properly understand these results, it is highlighted that the calculated $\dot{Q}_p$ includes also the term required to heat the air stream from T_e to T_s. This contri-bution ($= \dot{m}_a cp_a(T_s - T_e)/\eta_{th}$) is equal to 10.3 kW when T_e = 0 °C and to 6.6 kW when T_e = 10 °C, that is a significant fraction of the calculated $\dot{Q}_p$.

Although the proposed humidification system does not reach power savings (referred to the primary source) compared to steam to steam humidifiers, it is pointed out that *DWH* can be easily driven by waste heat or low grade heat from cogenerators. Instead such an option is not achievable with *SSH*, which requires high temperature heat to generate steam. Therefore the proposed

Table 6
Parameters used in the calculation of power consumption of reference technologies.

Parameter	*AH*	*ESH*	*SSH* 1	*SSH* 2
ΔP_{fil} (Pa)	150	150	150	150
ΔP_{HC} (Pa)	50	50	50	50
$\Delta P h_{um}$ (Pa)	50	30	30	30
η_{fan} (–)	0.7	0.7	0.7	0.7
η_{th} (–)	0.9	0.9	0.9	0.9
η_{el} (–)	0.525	0.525	0.525	0.525
$\eta_{th,v}$ (–)	–	–	0.8	0.6

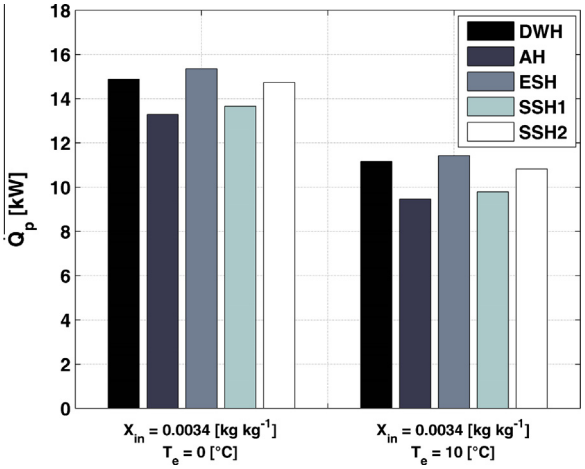

Fig. 17. $\dot{Q}_p$ of analyzed humidification systems in two different working conditions ($v_{reg,in}$ = 2 m s^{-1}, $v_{pro,in}$ = 2.6 m s^{-1}, $X_{reg,out}$ = 0.0066 kg kg^{-1}, N = 8 rev h^{-1}).

technology can be efficiently integrated in low temperature energy systems.

7. Conclusions

In this work a humidification system based on a desiccant wheel is proposed and it is investigated through a numerical and experimental approach. It is shown the system can properly provide an air stream at satisfactory humidity ratio through an appropriate arrangement of the desiccant wheel. The process air flow rate should be higher than the regeneration one: in most investigated cases, when $\dot{m}_{pro}/\dot{m}_{reg} > 1.3$, the desired outlet humidity can be achieved. In addition the lower the outdoor air temperature, the higher the process air flow rate. A critical issue is the outlet regeneration temperature, which can be too high (>30 °C) in particular working conditions and consequently can determine occupants' discomfort.

It has been highlighted that primary power consumption of the proposed system is lower than the one of electric steam humidifiers (up to −3%) and higher than the one of steam to steam humidifiers (up to +12%). Anyway, the humidification system based on desiccant wheel can be driven by low grade heat and it is appropriate to be integrated in innovative and efficient low temperature energy systems.

References

[1] ASHRAE Handbook. HVAC systems and equipment, American society of heating, refrigerating and air-conditioning engineers, Atlanta, USA; 2013.

[2] UNI 11425. Impianto di ventilazione e condizionamento a contaminazione controllata (VCCC) per il blocco operatorio – progettazione, installazione, messa in marcia, qualifica, gestione e manutenzione; 2011 [in Italian].

[3] De Antonellis S, Joppolo CM, Molinaroli L. Simulation, performance analysis and optimization of desiccant wheels. Energy Build 2010;42(9):1386–93.

[4] Angrisani G, Roselli C, Sasso M, Tariello F. Dynamic performance assessment of a micro-trigeneration system with a desiccant-based air handling unit in Southern Italy climatic conditions. Energy Convers Manage 2014;80 (April):188–201.

[5] El-Agouz SA, Kabeel AE. Performance of desiccant air conditioning system with geothermal energy under different climatic conditions. Energy Convers Manage 2014;88(December):464–75.

[6] Elgendy E, Mostafa A, Fatouh M. Performance enhancement of a desiccant evaporative cooling system using direct/indirect evaporative cooler. Int J Refrig 2015;51(March):77–87.

[7] Liu W, Lian Z, Radermacher R, Yao Y. Energy consumption analysis on a dedicated outdoor air system with rotary desiccant wheel. Energy 2007;32 (9):1749–60.

[8] Ruivo CR, Hernández FF, López JMC. Influence of the desiccant wheel effectiveness method approaches, with fix and variable effectiveness parameters, on the performance results of an airport air-conditioning system. Energy Convers Manage 2015;94(April):458–71.

[9] De Antonellis S, Joppolo CM, Molinaroli L, Pasini A. Simulation and energy efficiency analysis of desiccant wheel systems for drying processes. Energy 2012;37(1):336–45.

[10] Dai YJ, Wang RZ, Xu YX. Study of a solar powered solid adsorption–desiccant cooling system used for grain storage. Renewable Energy 2002;25(3):417–30.

[11] Wang WC, Calay RK, Chen YK. Experimental study of an energy efficient hybrid system for surface drying. Appl Therm Eng 2011;31(4):425–31.

[12] Guan Y, Zhang Y, Sheng Y, Kong X, Du S. Feasibility and economic analysis of solid desiccant wheel used for dehumidification and preheating in blast furnace. A case study of steel plant, Nanjing, China. Appl Therm Eng 2015;81 (25):426–35. April.

[13] Aprea C, Greco A, Maiorino A. The application of a desiccant wheel to increase the energetic performances of a transcritical cycle. Energy Convers Manage 2015;89(1):222–30. January.

[14] Sheng Y, Zhang Y, Zhang G. Simulation and energy saving analysis of high temperature heat pump coupling to desiccant wheel air conditioning system. Energy 2015;83(1):583–96. April.

[15] Fong KF, Chow TT, Lee CK, Lin Z, Chan LS. Solar hybrid cooling system for high-tech offices in subtropical climate – RAdiant cooling by absorption refrigeration and desiccant dehumidification. Energy Convers Manage 2011;52(8–9):2883–94.

[16] La D, Dai Y, Li H, Li Y, Kiplagat JK, Wang R. Experimental investigation and theoretical analysis of solar heating and humidification system with desiccant rotor. Energy Build 2011;43(5):1113–22.

[17] Zeng DQ, Li H, Dai YJ, Xie AX. Numerical analysis and optimization of a solar hybrid one-rotor two-stage desiccant cooling and heating system. Appl Therm Eng 2014;73(1):474–83.

[18] Rossi N. Manuale del termotecnico. 4th ed. Milano: Hoepli; 2014 [in Italian].

[19] De Antonellis S, Intini M, Joppolo CM, Pedranzini Federico. Experimental analysis and practical effectiveness correlations of enthalpy wheels. Energy Build 2014;84(December):316–23.

[20] De Antonellis S, Intini M, Joppolo CM. Desiccant wheels effectiveness parameters: correlations based on experimental data. Energy Build 2015;103 (September):296–306.

[21] DIN EN ISO 5167-2 Standards. Measurement of fluid flow by means of pressure differential devices inserted in circular cross-section conduits running full —Part 2: orifice plates (ISO 5167-2:2003).

[22] Sing KSW. Reporting physisorption data for gas/solid systems with special reference to the determination of surface area and porosity (Recommendations 1984). Pure Appl Chem 1985;57(4):603–19.

[23] Moffat RJ. Describing the uncertainties in experimental results. Exp Thermal Fluid Sci 1988;1(1):3–17.

[24] Aprile M, Motta M. Grey-box modelling and in situ experimental identification of desiccant rotors. Appl Therm Eng 2013;51(1–2):55–64.

[25] UNI 10339—Impianti aeraulici a fini di benessere—Generalità, classificazione e requisiti—Regole per la richiesta d'offerta, l'offerta, l'ordine e la fornitura; 1995.

[26] Intini M, De Antonellis S, Joppolo CM. The effect of inlet velocity and unbalanced flows on optimal working conditions of silica gel desiccant wheels. Energy Procedia 2014;48:858–64.

[27] ASHRAE. Indoor air quality; ashrae standard 62-2010; ASHRAE: Atlanta, GA, USA; 2011.